

## A NUMERICAL TECHNIQUE FOR SIMULATING VISCOELASTIC AXISYMMETRIC FREE SURFACE FLOWS

**Murilo F. Tomé** – murilo@lcad.icmc.sc.usp.br

**Luciane Grossi** – luciane@lcad.icmc.sc.usp.br

**Antonio Castelo Filho** – castelo@icmc.sc.usp.br

**José A. Cuminato** – jacumina@icmc.sc.usp.br

**Valdemir G. Ferreira** – valdemir@lcad.icmc.sc.usp.br

**Norberto Mangiavacchi** – norberto@lcad.icmc.usp.br

Universidade de São Paulo, Departamento de Ciências de Computação e Estatística

Cx.P. 668 – 13560-161 – São Carlos, SP, Brasil

**Sean McKee** – caas29@maths.strath.ac.uk

University of Strathclyde, Department of Mathematics

Glasgow, Scotland

**Abstract.** *This work deals with the development of a numerical method for simulating viscoelastic axisymmetric free surface flow of an Oldroyd-B fluid. The basic equations governing the flow of an Oldroyd-B fluid are considered. A novel formulation is developed for the computation of the extra-stress components on rigid boundaries and on the symmetry axis. The full free surface stress conditions are employed. The resulting governing equations are solved by the finite difference method on a MAC (Marker-And-Cell) grid. Numerical results demonstrating the capabilities of this new technique applied to axisymmetric flow of an Oldroyd-B fluid are presented for a number of problems involving unsteady free surface flows. In particular, the simulation of the extrudate swell of a highly elastic fluid is presented.*

**Keywords:** *Axisymmetric viscoelastic flow, Oldroyd-B, finite difference, constitutive equations.*

### 1. Introduction

Non-Newtonian free surface flows appear in many technological processes: container filling (food industry), injection moulding (plastic industries), ink jet devices, wire coating, among others, are all examples of non-Newtonian free surface flows problems. Today there is an intense activity in this area and many numerical techniques have been proposed over the past two decades to treat non-Newtonian flows. The models that have been studied tend to be the classical Oldroyd-B model or the upper convected Maxwell model with the constitutive equation either of differential or integral form. Numerical methods have included finite difference methods (eg. Yoo & Na 1991), finite element methods (eg. Marchal & Crochet 1987), Carew et al. 1993), Brasseur et al. 1998), finite volume methods (eg. Huang et al. 1996, Mompean & Deville 1997, Xue et al. 1998, Phillips & Williams 1999), spectral methods (eg. Beris et al. 1987), and boundary element methods (eg. Phan-Thien et al. 1991). Also, there now exists some measure of agreement for a class of test problems. These test problems have arisen because of the so called “High Weissenberg Number Problem”. Rather like the Reynolds number in Newtonian fluids, it has been found that a Weissenberg number is eventually reached above which convergence of the numerical method under consideration fails. And indeed this number was not very large and nearly all existing codes have difficulty with a Weissenberg number greater than about 4 (however, see Mompean & Deville 1997). In this paper viscoelastic axisymmetric flows with multiple free surfaces are considered. The approach employed is based upon the Marker-And-Cell (MAC) method of Harlow and Welch (Harlow & Welch 1970) and has been honed for many problems in Newtonian fluid mechanics (see eg. Tomé & McKee 1994, Tomé et al. 1996).

The method described herein is applied to tube flow and extrudate swell. Tube flow is employed to validate the numerical technique presented in this paper and the simulation of the extrudate swell demonstrates that our method can indeed simulate time-dependent free surface viscoelastic flows. The paper is organised as follows. The governing equations are set out in Section 2. The boundary conditions, specially for the non-Newtonian contribution to the extra-stress tensor, are discussed at length. The essence of the method is given in Section 3 while in Section 4, the basic finite difference discretisation is discussed. Section 5 includes some general comments and Section 6 provides numerical results; comparisons with other results and validation. Finally, Section 7 completes the paper with some concluding remarks.

### 2. Basic equations

The equations governing the flow of an Oldroyd-B fluid are (see Crochet, Davies & Walters 1984): the equation of motion and the mass conservation equation (assuming incompressibility)

$$\rho \frac{D\mathbf{u}}{Dt} = -\nabla p + \nabla \cdot \mathbf{T} + \rho \mathbf{g}; \quad \nabla \cdot \mathbf{u} = 0 \quad (1)$$

together with the constitutive equation

$$\mathbf{T} + \lambda_1 \overset{\nabla}{\mathbf{T}} = 2\mu_0 \left( \mathbf{D} + \lambda_2 \overset{\nabla}{\mathbf{D}} \right) \quad (2)$$

where  $\mathbf{T}$  is the symmetric extra-stress tensor. The upper convected derivative  $\overset{\nabla}{\mathbf{T}}$  is defined by

$$\overset{\nabla}{\mathbf{T}} = \frac{\partial \mathbf{T}}{\partial t} + (\mathbf{u} \cdot \nabla) \mathbf{T} - (\nabla \mathbf{u})^T \mathbf{T} - \mathbf{T} (\nabla \mathbf{u}) \quad \text{and} \quad \mathbf{D} = \frac{1}{2} \left( (\nabla \mathbf{u}) + (\nabla \mathbf{u})^T \right)$$

is the rate-of-deformation tensor and  $\lambda_1$  and  $\lambda_2$  are time constants (relaxation and retardation) and  $\mu_0$  is the viscosity. The vector  $\mathbf{u}$  denotes the velocity,  $p$  the pressure,  $\rho$  the density and  $\mathbf{g}$  the components of gravity.  $\frac{D}{Dt}$  denotes the material derivative. We observe that by making  $\lambda_2 = 0$  we obtain the Maxwell model. In order to solve (1)–(2) we perform the splitting

$$\mathbf{T} = 2\mu_0 \left( \frac{\lambda_2}{\lambda_1} \right) \mathbf{D} + \mathbf{S} \quad (3)$$

where  $\mathbf{S}$  represents the non-Newtonian contribution to the extra-stress tensor. By introducing (3) into (1) and (2) we obtain

$$\mathbf{S} + \lambda_1 \overset{\nabla}{\mathbf{S}} = 2\mu_0 \left( 1 - \frac{\lambda_2}{\lambda_1} \right) \mathbf{D} \quad (4)$$

$$\rho \frac{D\mathbf{u}}{Dt} = -\nabla p + 2\mu_0 \left( \frac{\lambda_2}{\lambda_1} \right) \nabla \cdot \mathbf{D} + \nabla \cdot \mathbf{S} + \rho \mathbf{g}. \quad (5)$$

We consider axisymmetric flows so that equations (4) and (5) can be written in the nondimensional form

$$\frac{1}{r} \frac{\partial}{\partial r}(ru) + \frac{\partial v}{\partial z} = 0, \quad (6)$$

$$\frac{\partial u}{\partial t} + \frac{1}{r} \frac{\partial(ru^2)}{\partial r} + \frac{\partial(uv)}{\partial z} = -\frac{\partial p}{\partial r} + \frac{1}{Re} \left( \frac{\lambda_2}{\lambda_1} \right) \left( \frac{1}{r} \frac{\partial}{\partial r} \left( r \frac{\partial u}{\partial r} \right) + \frac{\partial^2 u}{\partial z^2} - \frac{u}{r^2} \right) + \left( \frac{1}{r} \frac{\partial}{\partial r} (rS^{rr}) + \frac{\partial S^{rz}}{\partial z} - \frac{S^{\theta\theta}}{r} \right) + \frac{1}{Fr^2} g_r, \quad (7)$$

$$\frac{\partial v}{\partial t} + \frac{1}{r} \frac{\partial(ruv)}{\partial r} + \frac{\partial(v^2)}{\partial z} = -\frac{\partial p}{\partial z} + \frac{1}{Re} \left( \frac{\lambda_2}{\lambda_1} \right) \left( \frac{1}{r} \frac{\partial}{\partial r} \left( r \frac{\partial v}{\partial r} \right) + \frac{\partial^2 v}{\partial z^2} \right) + \left( \frac{1}{r} \frac{\partial}{\partial r} (rS^{rz}) + \frac{\partial S^{zz}}{\partial z} \right) + \frac{1}{Fr^2} g_z. \quad (8)$$

$$S^{rr} + We \left[ \frac{\partial S^{rr}}{\partial t} + \frac{1}{r} \frac{\partial(ruS^{rr})}{\partial r} + \frac{\partial(vS^{rr})}{\partial z} - 2 \frac{\partial u}{\partial r} S^{rr} - 2 \frac{\partial u}{\partial z} S^{rz} \right] = \frac{2}{Re} \left( 1 - \frac{\lambda_2}{\lambda_1} \right) \frac{\partial u}{\partial r}, \quad (9)$$

$$S^{\theta\theta} + We \left[ \frac{\partial S^{\theta\theta}}{\partial t} + \frac{1}{r} \frac{\partial(ruS^{\theta\theta})}{\partial r} + \frac{\partial(vS^{\theta\theta})}{\partial z} - 2 \frac{u}{r} S^{\theta\theta} \right] = \frac{2}{Re} \left( 1 - \frac{\lambda_2}{\lambda_1} \right) \frac{u}{r}, \quad (10)$$

$$S^{zz} + We \left[ \frac{\partial S^{zz}}{\partial t} + \frac{1}{r} \frac{\partial(ruS^{zz})}{\partial r} + \frac{\partial(vS^{zz})}{\partial z} - 2 \frac{\partial v}{\partial r} S^{rz} - 2 \frac{\partial v}{\partial z} S^{zz} \right] = \frac{2}{Re} \left( 1 - \frac{\lambda_2}{\lambda_1} \right) \frac{\partial v}{\partial z}, \quad (11)$$

$$S^{rz} + We \left[ \frac{\partial S^{rz}}{\partial t} + \frac{1}{r} \frac{\partial(ruS^{rz})}{\partial r} + \frac{\partial(vS^{rz})}{\partial z} - \frac{\partial v}{\partial r} S^{rr} + \frac{u}{r} S^{rz} - \frac{\partial u}{\partial z} S^{zz} \right] = \frac{1}{Re} \left( 1 - \frac{\lambda_2}{\lambda_1} \right) \left( \frac{\partial u}{\partial z} + \frac{\partial v}{\partial r} \right), \quad (12)$$

respectively, where  $Re = UL/\nu_0$  denotes the Reynolds number,  $We = \lambda_1(U/L)$  is the Weissenberg number,  $Fr = U/\sqrt{Lg}$  is the Froude number.  $L$ ,  $U$  and  $\nu_0$  denote “typical” length, velocity and viscosity scales, respectively.

### 3. Boundary Conditions

In order to solve (6)–(12) the values of  $\mathbf{u}$  and  $\mathbf{S}$  on the boundary are required. For the momentum equations it is sufficient that we have  $\mathbf{u} = 0$  on rigid boundaries.

#### 3.1 Computation of the stress on rigid boundaries

As rigid boundaries may be regarded as characteristics, the stresses  $S^{rr}$ ,  $S^{\theta\theta}$ ,  $S^{zz}$  and  $S^{rz}$  on the boundary may be computed from (9)–(12), which we assume to hold on rigid boundaries with the initial condition  $\mathbf{S} = \mathbf{0}$ . We make the change of variables:  $\mathbf{S} = e^{-\frac{1}{We}t} \tilde{\mathbf{S}}$  which introduced into (10)–(12) yields the following equations

$$\frac{\partial \tilde{S}^{rr}}{\partial t} = -\frac{1}{r} \frac{\partial(ru\tilde{S}^{rr})}{\partial r} - \frac{\partial(v\tilde{S}^{rr})}{\partial z} + 2 \frac{\partial u}{\partial r} \tilde{S}^{rr} + 2 \frac{\partial u}{\partial z} \tilde{S}^{rz} + \frac{1}{We} \frac{2}{Re} e^{\frac{1}{We}t} \left( 1 - \frac{\lambda_2}{\lambda_1} \right) \frac{\partial u}{\partial r} \quad (13)$$

$$\frac{\partial \tilde{S}^{\theta\theta}}{\partial t} = -\frac{1}{r} \frac{\partial(ru\tilde{S}^{\theta\theta})}{\partial r} - \frac{\partial(v\tilde{S}^{\theta\theta})}{\partial z} + 2 \frac{u}{r} \tilde{S}^{\theta\theta} + \frac{1}{We} \frac{2}{Re} e^{\frac{1}{We}t} \left( 1 - \frac{\lambda_2}{\lambda_1} \right) \frac{u}{r}, \quad (14)$$

$$\frac{\partial \tilde{S}^{zz}}{\partial t} = -\frac{1}{r} \frac{\partial(ru\tilde{S}^{zz})}{\partial r} - \frac{\partial(v\tilde{S}^{zz})}{\partial z} + 2\frac{\partial v}{\partial r}\tilde{S}^{rz} + 2\frac{\partial v}{\partial z}\tilde{S}^{zz} + \frac{1}{We} \frac{2}{Re} e^{\frac{1}{We}} \left(1 - \frac{\lambda_2}{\lambda_1}\right) \frac{\partial v}{\partial z}, \quad (15)$$

$$\frac{\partial \tilde{S}^{rz}}{\partial t} = -\frac{1}{r} \frac{\partial(ru\tilde{S}^{rz})}{\partial r} - \frac{\partial(v\tilde{S}^{rz})}{\partial z} + \frac{\partial v}{\partial r}\tilde{S}^{rr} + \frac{\partial u}{\partial z}\tilde{S}^{zz} - \frac{u}{r}\tilde{S}^{rz} + \frac{1}{We} \frac{1}{Re} e^{\frac{1}{We}} \left(1 - \frac{\lambda_2}{\lambda_1}\right) \left(\frac{\partial u}{\partial z} + \frac{\partial v}{\partial r}\right), \quad (16)$$

Equations (13)-(16) can be solved for the components of the non-Newtonian stress tensor on rigid boundaries which are parallel to the  $z$ -axis or parallel to the  $r$ -axis. It can be shown (see Tome et al. 2002) that on rigid boundaries which are parallel to the  $r$ -axis, the expressions for the components of the non-Newtonian extra stress tensor are given by

$$S^{rr}(r, z, t + \delta t) = e^{\frac{-1}{We}\delta t} S^{rr}(r, z, t) + \delta t \left[ \frac{\partial u}{\partial z}(r, z, t) e^{\frac{-1}{We}\delta t} S^{rz}(r, z, t) + \frac{\partial u}{\partial z}(r, z, t + \delta t) S^{rz}(r, z, t + \delta t) \right], \quad (17)$$

$$S^{\theta\theta}(r, z, t + \delta t) = 0, \quad S^{zz}(r, z, t + \delta t) = 0, \quad (18)$$

$$S^{rz}(r, z, t + \delta t) = e^{\frac{-1}{We}\delta t} \tilde{S}^{rz}(r, z, t) + \frac{1}{Re} \left(1 - \frac{\lambda_2}{\lambda_1}\right) \frac{\partial u}{\partial z}(r, z, t^*) \left[1 - e^{\frac{-1}{We}\delta t}\right]. \quad (19)$$

The calculation of the components of the non-Newtonian extra stress on rigid boundaries which are parallel to the  $z$ -axis is performed in a similar manner as for rigid boundaries parallel to the  $r$ -axis.

### 3.2 Computation of the stress components on the symmetry axis

Following the same ideas employed for the computation of the non-Newtonian extra stress on rigid boundaries, one can show that on the symmetry axis, the components of the non-Newtonian extra stress are given by

$$S^{\theta\theta}(t) = 0, \quad S^{rz}(t) = 0, \quad (20)$$

$$S^{rr}(t + \delta t) = e^{\frac{-1}{We}\delta t} S^{rr}(t) - \frac{\delta t}{2} \left( \left. \frac{\partial v S^{rr}}{\partial z} \right|_{t+\delta t} + e^{\frac{-1}{We}\delta t} \left. \frac{\partial v S^{rr}}{\partial z} \right|_t \right) + \delta t \left( \left. \frac{\partial u}{\partial r} \right|_{t+\delta t} S^{rr} \right|_{t+\delta t} + e^{\frac{-1}{We}\delta t} \left. \frac{\partial u}{\partial r} \right|_t S^{rr} \right|_t \right) + \frac{2}{Re} \left(1 - \frac{\lambda_2}{\lambda_1}\right) \left. \frac{\partial u}{\partial r} \right|_{t=t^*} \left(1 - e^{\frac{-1}{We}\delta t}\right), \quad (21)$$

$$S^{zz}(t + \delta t) = e^{\frac{-1}{We}\delta t} S^{zz}(t) - \frac{\delta t}{2} \left( \left. \frac{\partial v S^{zz}}{\partial z} \right|_{t+\delta t} + e^{\frac{-1}{We}\delta t} \left. \frac{\partial v S^{zz}}{\partial z} \right|_t \right) + \delta t \left( \left. \frac{\partial v}{\partial z} \right|_{t+\delta t} S^{zz} \right|_{t+\delta t} + e^{\frac{-1}{We}\delta t} \left. \frac{\partial v}{\partial z} \right|_t S^{zz} \right|_t \right) + \frac{2}{Re} \left(1 - \frac{\lambda_2}{\lambda_1}\right) \left. \frac{\partial v}{\partial z} \right|_{t=t^*} \left(1 - e^{\frac{-1}{We}\delta t}\right). \quad (22)$$

### 3.3 Inflow and Outflow boundaries

At the fluid entrance we specify the velocity components  $u_n = U$  and  $u_\tau = 0$  while for the non-Newtonian extra stress tensor components  $S_{ik}$  we follow the strategy of Mompean and Deville (see Mompean & Deville 1997) and set  $S^{rr} = 0$ ,  $S^{\theta\theta} = 0$ ,  $S^{rz} = 0$  and  $S^{zz} = 0$ . At fluid exit we impose homogeneous Neumann conditions for both the velocity components and the extra stress components, namely:

$$\frac{\partial u_n}{\partial n} = \frac{\partial u_\tau}{\partial n} = \frac{\partial S^{rr}}{\partial n} = \frac{\partial S^{rz}}{\partial n} = \frac{\partial S^{\theta\theta}}{\partial n} = \frac{\partial S^{zz}}{\partial n} = 0. \quad (23)$$

In the equations above the subscripts  $n$  and  $\tau$  denote directions normal and tangential to the boundary, respectively.

### 3.4 Free Surface Stress Conditions

We shall consider unsteady free-surface flows of a viscous fluid moving into a passive atmosphere (which we may take to be at zero pressure). In the absence of surface tension the normal and tangential components of stress must be continuous across any free surface, so that on such a surface (see Tomé et al. 2002)

$$-p + \frac{2}{Re} \left[ \left(\frac{\lambda_2}{\lambda_1}\right) \left( \frac{\partial u}{\partial r} n_r^2 + \left( \frac{\partial u}{\partial z} + \frac{\partial v}{\partial r} \right) n_z n_r + \frac{\partial v}{\partial z} n_z^2 \right) \right] + S^{rr} n_r^2 + 2S^{zr} n_r n_z + S^{zz} n_z^2 = 0, \quad (24)$$

$$\frac{1}{Re} \left(\frac{\lambda_2}{\lambda_1}\right) \left[ 2 \left( \frac{\partial v}{\partial z} - \frac{\partial u}{\partial r} \right) n_r n_z + \left( \frac{\partial u}{\partial z} + \frac{\partial v}{\partial r} \right) (n_r^2 - n_z^2) \right] + (S^{zz} - S^{rr}) n_r n_z + S^{zr} (n_r^2 - n_z^2) = 0. \quad (25)$$

where  $\mathbf{n} = (n_r, n_z)$  is the outward normal vector to the surface. Equations (24)–(25) are used to compute the pressure  $\tilde{p}$  and the velocities on the free surface taking into account the local orientation of the fluid surface. They are approximated by finite difference equations following the ideas of (Tomé et al. 2002).

#### 4. Method of Solution

To solve equations (6)–(12) we employ a procedure similar to that introduced by (Tomé et al. 2002).

Let us suppose that at a given time, say  $t_n$ , the velocity field  $\mathbf{u}(r, z, t_n)$  and the non-Newtonian extra stress tensor  $\mathbf{S}(r, z, t_n)$  are known and the values of  $\mathbf{u}$ ,  $\mathbf{S}$  and  $p$  are given on specified parts of the boundary. To compute the velocity field, pressure field and the non-Newtonian extra-stress tensor at the advanced time  $t_{n+1} = t_n + \delta t$ , we proceed as follows:

**Step 1:** Let  $\tilde{p}$  be a pressure field which satisfies the correct pressure condition on the free surface. This pressure field is computed from the stress conditions (24).

**Step 2:** Calculate the intermediate velocity field,  $\tilde{\mathbf{u}}(r, z, t_{n+1})$ , from

$$\frac{\partial u}{\partial t} = \frac{1}{r} \frac{\partial(ru^2)}{\partial r} + \frac{\partial(uv)}{\partial z} - \frac{\partial p}{\partial r} + \frac{1}{Re} \left( \frac{\lambda_2}{\lambda_1} \right) \left[ \frac{1}{r} \frac{\partial}{\partial r} \left( r \frac{\partial u}{\partial r} \right) + \frac{\partial^2 u}{\partial z^2} - \frac{u}{r^2} \right] + \left[ \frac{1}{r} \frac{\partial}{\partial r} (rS^{rr}) + \frac{\partial S^{zr}}{\partial z} - \frac{S^{\theta\theta}}{r} \right] + \frac{1}{Fr^2} g_r, \quad (26)$$

$$\frac{\partial v}{\partial t} = \frac{1}{r} \frac{\partial(ruv)}{\partial r} + \frac{\partial(v^2)}{\partial z} - \frac{\partial p}{\partial z} + \frac{1}{Re} \left( \frac{\lambda_2}{\lambda_1} \right) \left[ \frac{1}{r} \frac{\partial}{\partial r} \left( r \frac{\partial v}{\partial r} \right) + \frac{\partial^2 v}{\partial z^2} \right] + \left[ \frac{1}{r} \frac{\partial}{\partial r} (rS^{rz}) + \frac{\partial S^{zz}}{\partial z} \right] + \frac{1}{Fr^2} g_z, \quad (27)$$

with  $\tilde{\mathbf{u}}(r, z, t_n) = \mathbf{u}(r, z, t_n)$  using the correct boundary conditions for  $\mathbf{u}(r, z, t_n)$ . These equations are solved by a finite difference method which is usually, but not necessarily, explicit.

**Step 3:** Solve the Poisson equation:  $\nabla^2 \psi(r, z, t_{n+1}) = \nabla \cdot \tilde{\mathbf{u}}(r, z, t_{n+1})$ . The appropriate boundary conditions for this equation are (see Tomé et al. [25]):  $\frac{\partial \psi}{\partial n} = 0$  on rigid boundaries and  $\psi = 0$  on the free surface.

**Step 4:** Compute the velocity field:  $\mathbf{u}(r, z, t_{n+1}) = \tilde{\mathbf{u}}(r, z, t_{n+1}) - \nabla \psi(r, z, t_{n+1})$ .

**Step 5:** Compute the pressure:  $p(\mathbf{x}, t_{n+1}) = \tilde{p}(\mathbf{x}, t_n) + \frac{\psi(\mathbf{x}, t_{n+1})}{\delta t}$ .

**Step 6:** Update the components of the non-Newtonian extra-stress tensor on rigid boundaries according to the equations given in Section 3.1.

**Step 7:** Update the components of the non-Newtonian extra-stress tensor on the symmetry axis according to the equations given in Section 3.2.

**Step 8:** Compute the components of the non-Newtonian extra-stress tensor,  $S^{rr}(\mathbf{x}, t_{n+1}), \dots, S^{rz}(\mathbf{x}, t_{n+1})$ , from:

$$S^{rr} + We \left[ \frac{\partial S^{rr}}{\partial t} + \frac{1}{r} \frac{\partial(ruS^{rr})}{\partial r} + \frac{\partial(vS^{rr})}{\partial z} - 2 \frac{\partial u}{\partial r} S^{rr} - 2 \frac{\partial u}{\partial z} S^{rz} \right] = \frac{2}{Re} \left( 1 - \frac{\lambda_2}{\lambda_1} \right) \frac{\partial u}{\partial r}, \quad (28)$$

$$S^{\theta\theta} + We \left[ \frac{\partial S^{\theta\theta}}{\partial t} + \frac{1}{r} \frac{\partial(ruS^{\theta\theta})}{\partial r} + \frac{\partial(vS^{\theta\theta})}{\partial z} - 2 \frac{u}{r} S^{\theta\theta} \right] = \frac{2}{Re} \left( 1 - \frac{\lambda_2}{\lambda_1} \right) \frac{u}{r}, \quad (29)$$

$$S^{zz} + We \left[ \frac{\partial S^{zz}}{\partial t} + \frac{1}{r} \frac{\partial(ruS^{zz})}{\partial r} + \frac{\partial(vS^{zz})}{\partial z} - 2 \frac{\partial v}{\partial r} S^{rz} - 2 \frac{\partial v}{\partial z} S^{zz} \right] = \frac{2}{Re} \left( 1 - \frac{\lambda_2}{\lambda_1} \right) \frac{\partial v}{\partial z}, \quad (30)$$

$$S^{rz} + We \left[ \frac{\partial S^{rz}}{\partial t} + \frac{1}{r} \frac{\partial(ruS^{rz})}{\partial r} + \frac{\partial(vS^{rz})}{\partial z} - \frac{\partial v}{\partial r} S^{rr} + \frac{u}{r} S^{rz} - \frac{\partial u}{\partial z} S^{zz} \right] = \frac{1}{Re} \left( 1 - \frac{\lambda_2}{\lambda_1} \right) \left( \frac{\partial u}{\partial z} + \frac{\partial v}{\partial r} \right). \quad (31)$$

Equations (28)–(31) are solved by finite differences. Details of the difference equations are given in the next Section.

**Step 9:** Update the markers positions: The last step in the calculation is to move the markers to their new positions. This is done by solving

$$\frac{dx}{dt} = u, \quad \frac{dy}{dt} = v, \quad (32)$$

for each particle. The fluid surface is defined by a list containing these markers and the visualization of the free surface is obtained simply by connecting them by straight lines.

#### 5. Finite Difference Approximation

As the fluid is continuously moving, a procedure for identifying the fluid region and the free surface needs to be described. To effect this, the cells within the mesh are flagged as: Empty (E) - Cells that do not contain fluid; Full (F) - Cells full of fluid. These cells do not have any face contiguous with an Empty cell; Surface (S) - Cells that contain fluid and have at least one face contiguous with an Empty cell face. These cells contain the free surface; Boundary (B) - Cells that define a rigid boundary. In these cells the no-slip condition is applied; Inflow (I) - Cells that define an inflow boundary and Outflow (O) - Cells that define an outflow boundary. Figure 1 illustrates the cell structure for a two-dimensional flow at a given instant of time. For clarity, the empty cells are left blank.

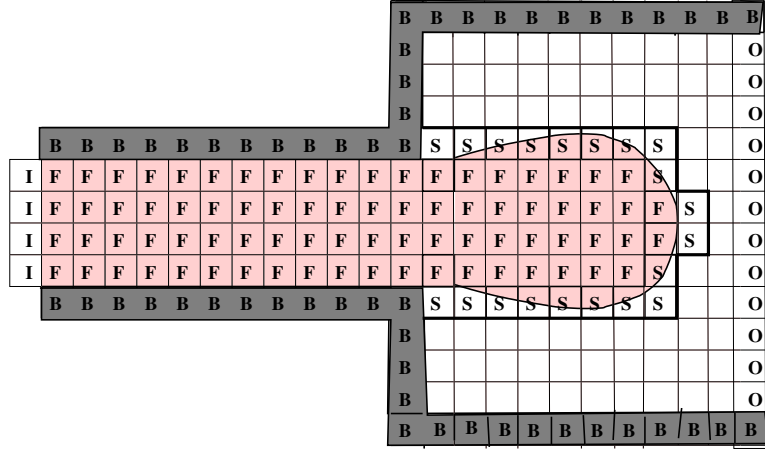


Fig. 1. Types of cells used in a GENSMAC calculation.

Equations (26)–(31) will be solved by a finite difference method on a staggered grid. The components of the non-Newtonian extra-stress tensor together with the pressure field are applied at the centre of a cell while the velocity components  $u$  and  $v$  are staggered by  $\delta r/2$  and  $\delta z/2$ , respectively. The momentum equations (26)–(27) are approximated by finite differences as follows: the time derivative is modeled by the Euler method. The linear spatial terms are approximated by central differences while for the convective terms we employ a high order upwind method. In this work we have used the VONOS method (see Ferreira et al. 2002). Details of the finite difference implementation of this high order upwind scheme are given in (Ferreira et al. 2002). Thus, the momentum equations (26) – (27) are approximated by

$$\begin{aligned} \tilde{u}_{i+\frac{1}{2},j}^{n+1} = & u_{i+\frac{1}{2},j} + \delta t \left[ -\frac{1}{r_{i+\frac{1}{2}}} \mathbf{conv}(ru^2) - \mathbf{conv}(vu) - \frac{\tilde{p}_{i+1,j} - \tilde{p}_{i,j}}{\delta r} + \frac{1}{Re} \left( \frac{\lambda_2}{\lambda_1} \right) \left( \frac{1}{r_{i+\frac{1}{2}}} \frac{(r_i u_{i-\frac{1}{2},j})}{r_{i+\frac{1}{2}}} \right. \right. \\ & \left. \left. - \frac{(r_i + r_{i+1})u_{i+\frac{1}{2},j} + r_{i+1}u_{i+\frac{3}{2},j}}{\delta r^2} + \frac{(u_{i+\frac{1}{2},j-1} - 2u_{i+\frac{1}{2},j} + u_{i+\frac{1}{2},j+1})}{\delta z} - \frac{u_{i+\frac{1}{2},j}}{r_{i+\frac{1}{2}}^2} \right) \right. \\ & \left. \frac{1}{r_{i+\frac{1}{2}}} \frac{(r_{i+1}S_{i+1,j}^{rr} - r_i S_{i,j}^{rr})}{\delta r} + \frac{S_{i+\frac{1}{2},j+\frac{1}{2}}^{rz} - S_{i+\frac{1}{2},j-\frac{1}{2}}^{rz}}{\delta z} + \frac{(S_{i+1,j}^{\theta\theta} + S_{i,j}^{\theta\theta})}{2} + \frac{1}{F_r^2} g_r \right], \end{aligned} \quad (33)$$

$$\begin{aligned} \tilde{v}_{i,j+\frac{1}{2}}^{n+1} = & v_{i,j+\frac{1}{2}} + \delta t \left[ -\frac{1}{r_i} \mathbf{conv}(ruv) - \mathbf{conv}(v^2) - \frac{\tilde{p}_{i,j+1} - \tilde{p}_{i,j}}{\delta z} + \frac{1}{Re} \left( \frac{\lambda_2}{\lambda_1} \right) \left( \frac{1}{r_i} \frac{(r_{i-\frac{1}{2}} v_{i-1,j+\frac{1}{2}})}{r_i} \right. \right. \\ & \left. \left. - \frac{(r_{i+\frac{1}{2}} + r_{i-\frac{1}{2}})v_{i,j+\frac{1}{2}} + r_{i+\frac{1}{2}}v_{i+1,j+\frac{1}{2}}}{\delta r^2} + \frac{(v_{i,j-\frac{1}{2}} - 2v_{i,j+\frac{1}{2}} + v_{i,j+\frac{3}{2}})}{\delta z} \right) \right. \\ & \left. \frac{1}{r_i} \frac{(r_{i+\frac{1}{2}} S_{i+\frac{1}{2},j+\frac{1}{2}}^{rz} - r_{i-\frac{1}{2}} S_{i-\frac{1}{2},j+\frac{1}{2}}^{rz})}{\delta r} + \frac{S_{i,j+1}^{zz} - S_{i,j}^{zz}}{\delta z} + \frac{1}{F_r^2} g_z \right]. \end{aligned} \quad (34)$$

In a similar manner, the components of the non-Newtonian tensor (28)–(31) are approximated by finite differences. Again, the convective terms are modeled by the high order VONOS method (see Ferreira et al. 2002). Thus, equations (28)–(31) are approximated by

$$\begin{aligned} S_{i,j}^{rr(n+1)} = & \left( 1 - \frac{\delta t}{We} \right) S_{i,j}^{rr} - \delta t \left[ \frac{1}{r_i} \mathbf{conv}(ruS^{rr})_{i,j} + \mathbf{conv}(vS^{rr})_{i,j} - 2 \frac{(u_{i+\frac{1}{2},j} - u_{i-\frac{1}{2},j})}{\delta r} S_{i,j}^{rr} \right. \\ & \left. - 2 \frac{(u_{i,j+\frac{1}{2}} - u_{i,j-\frac{1}{2}})}{\delta z} S_{i,j}^{rz} + \frac{1}{Re} \frac{2}{We} \left( \frac{\lambda_2}{\lambda_1} - 1 \right) \frac{(u_{i+\frac{1}{2},j} - u_{i-\frac{1}{2},j})}{\delta r} \right] \end{aligned} \quad (35)$$

$$\begin{aligned} S_{i,j}^{\theta\theta(n+1)} = & \left( 1 - \frac{\delta t}{We} \right) S_{i,j}^{\theta\theta} - \delta t \left[ \frac{1}{r_i} \mathbf{conv}(ruS^{\theta\theta})_{i,j} + \mathbf{conv}(vS^{\theta\theta})_{i,j} - \frac{1}{r_i} (u_{i+\frac{1}{2},j} - u_{i-\frac{1}{2},j}) S_{i,j}^{\theta\theta} \right. \\ & \left. + \frac{1}{Re} \frac{2}{We} \left( \frac{\lambda_2}{\lambda_1} - 1 \right) \frac{(u_{i+\frac{1}{2},j} + u_{i-\frac{1}{2},j})}{r_i} \right] \end{aligned} \quad (36)$$

$$\begin{aligned} S_{i,j}^{zz(n+1)} = & \left( 1 - \frac{\delta t}{We} \right) S_{i,j}^{zz} - \delta t \left[ \frac{1}{r_i} \mathbf{conv}(ruS^{zz})_{i,j} + \mathbf{conv}(vS^{zz})_{i,j} - 2 \frac{(v_{i,j+\frac{1}{2}} - v_{i,j-\frac{1}{2}})}{\delta z} S_{i,j}^{zz} \right. \\ & \left. - 2 \frac{(v_{i+\frac{1}{2},j} - v_{i-\frac{1}{2},j})}{\delta r} S_{i,j}^{rz} + \frac{1}{Re} \frac{2}{We} \left( \frac{\lambda_2}{\lambda_1} - 1 \right) \frac{(v_{i,j+\frac{1}{2}} - v_{i,j-\frac{1}{2}})}{\delta z} \right] \end{aligned} \quad (37)$$

$$\begin{aligned}
S_{i,j}^{rz(n+1)} = & \left(1 - \frac{\delta t}{We}\right) S_{i,j}^{rz} - \delta t \left[ \frac{1}{r_i} \mathbf{conv}(ruS^{rz})_{i,j} + \mathbf{conv}(vS^{rz})_{i,j} - \frac{(v_{i+\frac{1}{2},j} - v_{i-\frac{1}{2},j})}{\delta r} S_{i,j}^{rr} \right. \\
& - \frac{(u_{i,j+\frac{1}{2}} - u_{i,j-\frac{1}{2}})}{\delta z} S_{i,j}^{zz} + \frac{1}{Re} \frac{1}{We} \left( \frac{\lambda_2}{\lambda_1} - 1 \right) \left( \frac{u_{i,j+\frac{1}{2}} - u_{i,j-\frac{1}{2}}}{\delta z} + \frac{v_{i+\frac{1}{2},j} - v_{i-\frac{1}{2},j}}{\delta r} \right) \\
& \left. - \frac{1}{r_i} \frac{(u_{i+\frac{1}{2},j} + u_{i-\frac{1}{2},j})}{2} S_{i,j}^{rz} \right]
\end{aligned} \tag{38}$$

In equations (33)–(38), terms which are not defined at the cell position given by their subscripts are obtained by averaging, that is:

$$\begin{aligned}
u_{i,j+\frac{1}{2}} & := \frac{u_{i+\frac{1}{2},j} + u_{i+\frac{1}{2},j+1} + u_{i-\frac{1}{2},j} + u_{i-\frac{1}{2},j+1}}{4}, & v_{i+\frac{1}{2},j} & := \frac{v_{i,j+\frac{1}{2}} + v_{i+1,j+\frac{1}{2}} + v_{i,j-\frac{1}{2}} + v_{i+1,j-\frac{1}{2}}}{4}, \\
S_{i+\frac{1}{2},j+\frac{1}{2}}^{rz} & := \frac{S_{i,j}^{rz} + S_{i+1,j}^{rz} + S_{i,j+1}^{rz} + S_{i+1,j+1}^{rz}}{4}.
\end{aligned}$$

The Poisson equation (see **step 3**) in cylindrical coordinates becomes can be written in the form

$$\frac{\partial}{\partial r} \left( r \frac{\partial \psi}{\partial r} \right) + r \frac{\partial^2 \psi}{\partial z^2} = r \tilde{D} \tag{39}$$

and discretizing (39) at the cell centre we obtain (assuming  $\delta r = \delta z$ )

$$-r_i \psi_{i,j-1} - r_{i-\frac{1}{2}} \psi_{i-1,j} + 4r_i \psi_{i,j} - r_{i+\frac{1}{2}} \psi_{i+1,j} - r_i \psi_{i,j+1} = -r_i \delta r^2 \tilde{D}_{i,j} \tag{40}$$

where

$$\tilde{D}_{i,j} = \frac{1}{r_i} \left( \frac{r_{i+\frac{1}{2}} \tilde{u}_{i+\frac{1}{2},j} - r_{i-\frac{1}{2}} \tilde{u}_{i-\frac{1}{2},j}}{\delta r} \right) + \frac{\tilde{v}_{i,j+\frac{1}{2}} - \tilde{v}_{i,j-\frac{1}{2}}}{\delta z}.$$

Equation (40) leads to a symmetric and positive definite linear system for  $\psi_{i,j}$ . In order to solve this linear system we employ the conjugate gradient method as implemented in GENSMAC (see Tomé and McKee 1994). The final velocities are obtained by discretizing (see **Step 4**) at the respective nodes, namely

$$u_{i+\frac{1}{2},j}^{n+1} = \tilde{u}_{i+\frac{1}{2},j} - \left( \frac{\psi_{i+1,j} - \psi_{i,j}}{\delta x} \right), \quad v_{i,j+\frac{1}{2}}^{n+1} = \tilde{v}_{i,j+\frac{1}{2}} - \left( \frac{\psi_{i,j+1} - \psi_{i,j}}{\delta y} \right). \tag{41}$$

The pressure is obtained by applying (see **Step 5**) at the cell centres, giving:

$$p_{i,j} = \tilde{p}_{i,j} + \frac{\psi_{i,j}}{\delta t} \tag{42}$$

Consequently, each calculational cycle consists of solving equations (33)–(38) and (40)–(42) at each time-step.

## 6. Validation and Numerical Results

The finite difference equations described in this paper have been implemented into the GENSMAC code (see Tomé & McKee 1994) in order to simulate free surface flow of an Oldroyd-B fluid. The discretized momentum equations are solved by the GENSMAC code; it was only necessary to modify the routine to include the terms involving the non-Newtonian component of the extra-stress tensor. The discretized Poisson equation (40) is solved by the conjugate gradient method as implemented in the GENSMAC code. The equations for calculating the final velocities and the pressure equation are solved as in the GENSMAC code as they do not differ from those for a Newtonian fluid. A number of routines have been written to set up the boundary conditions on inflows, outflows, rigid boundaries and free surface.

### 6.1 Validation of the approach: numerical simulation of the flow in a pipe.

We validate the approximation of the viscoelastic extra-stress tensor on rigid boundaries, on the symmetry axis and on interior points by simulating the flow in a pipe. We consider a pipe of diameter  $2R$  and having a length of  $10R$  (see figure 2a). At the pipe entrance we impose the analytic fully developed flow profiles for the velocity and the non-Newtonian extra stress. At the exit the conditions described in this paper for outflow boundaries are assumed (see Section 3.3). The computational domain is shown in figure 2b. On the pipe wall (see figure 2b) the no-slip condition and the expressions for the components of the viscoelastic extra-stress tensor (see Section 3.1) are applied while on the symmetry line the equations derived in Section 3.2 are employed. We start with the pipe empty and inject fluid at the inflow at a prescribed velocity. The fully developed flow profiles imposed at the inflow are given by

$$v(r) = \frac{2(R^2 - r^2)}{R^2}, \quad u = 0 \tag{43}$$

$$S^{rz} = \frac{1}{Re} \left( 1 - \frac{\lambda_2}{\lambda_1} \right) \left( \frac{\partial v}{\partial r} \right), \quad S^{zz}(r) = 2WeS^{rz} \left( \frac{\partial v}{\partial r} \right), \quad S^{\theta\theta} = S^{rr} = 0. \tag{44}$$

Initially the pipe is empty and fluid is injected at the inflow until it reaches the outflow and steady state is established. Under steady state conditions the velocity field and the viscoelastic extra-stress in the pipe must have the same values as those of the inflow. To verify this, we performed two simulations using  $We = 1$  and  $We = 1.5$ . The input data used were  $L = R = 1$ ,  $U = 1$ ,  $\delta r = \delta z = 0.1$ ,  $\nu = 1$ . The time constant  $\lambda_1$  took the values of  $\lambda_1 = 1$  and  $\lambda_1 = 1.5$ ; the ratio  $\lambda_2/\lambda_1$  was set equal to 0.5. In these runs we have  $Re = LU/\nu = 1$  and  $We = \lambda_1 U/L = 1, 1.5$ . Figure 3 presents several snapshots taken from the simulation with  $We = 1$  at different times, showing the fluid filling the tube. Figure 3d displays the steady state fluid velocity at time  $t = 25.0$ . Figure 4 displays the values of the non-Newtonian extra-stress components  $S^{rz}$  and  $S^{rr}$  at the line  $z = 5$  (middle of the pipe) with  $We = 1$ ; the respective analytic values (see eq. (44)) are also shown. The solid lines in figure 4 are the analytic solutions while the dotted lines and the dotted-dashed lines are the numerical solutions for the extra-stress components, respectively. The results of the simulation with  $We = 1.5$  are displayed in figure 5. As can be seen from figures 4 and 5 the agreement between the exact and the numerical solutions is very good. Indeed, the relative  $l_2$ -norm of the errors,

$$E^{rz} = \frac{\sum (S_{exact}^{rz} - S_{numerical}^{rz})^2}{\sum (S_{exact}^{rz})^2}, \quad E^{rr} = \frac{\sum (S_{exact}^{rr} - S_{numerical}^{rr})^2}{\sum (S_{exact}^{rr})^2}$$

are  $E^{rz} = 0.0000143$  and  $E^{zz} = 0.0000576$  for  $We = 1$  and  $E^{rz} = 0.0000079$  and  $E^{rr} = 0.0000471$  for  $We = 1.5$

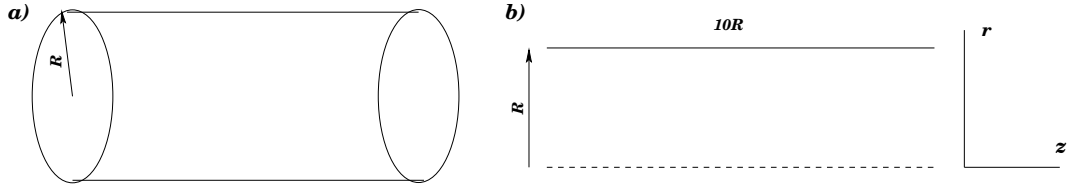


Fig. 2. Pipe flow set up parameters.

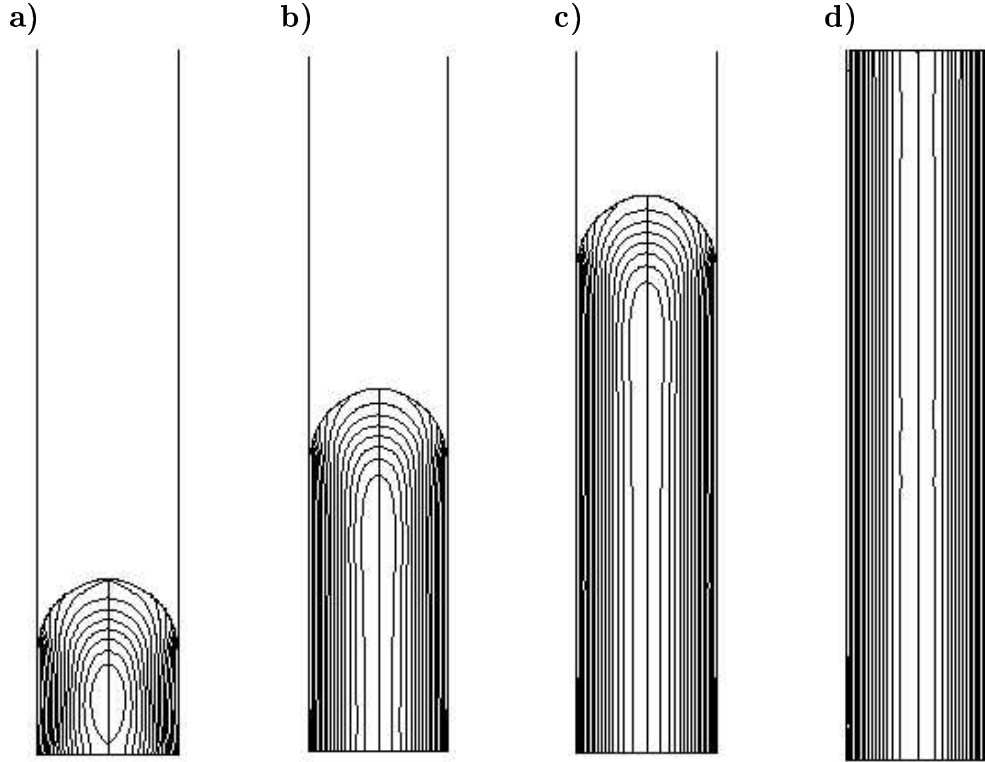


Fig. 3. Numerical simulation of pipe flow. Fluid surface and velocity contours at times: a)  $t = 2.0$ , b)  $t = 4.5$ , c)  $t = 7.0$  and d)  $t = 24.5$ .

## 6.2 Numerical simulation of the transient extrudate swell of an axisymmetric jet

We present a simulation of the flow of a jet emerging from a tube which exhibits the characteristic phenomenon known as “extrudate swell” or “jet swell”. This problem has attracted the attention of many researchers and various techniques for its simulation have been proposed (e.g. Brasseur et al. 1998, Crochet, Davies & Walters 1984), Crochet & Keunings 1982, Crochet & Keunings 1980).

We consider the time-dependent flow of an axisymmetric jet flowing through a tube and extruding into air. The no-slip condition is imposed on the wall of the tube while full developed flow is imposed at the fluid entrance (see equations

(43) and (44)). On the fluid free surface we imposed the full stress conditions (see (24) and (25)). The components of the non-Newtonian stress  $\mathbf{S}$  on the wall tube and on the symmetry line are computed according to the equations derived in Sections 3.1 and 3.2, respectively. The flow domain is the same as that of figure 2. The following input data were employed:

- Tube length:  $L = 5R = 5$  cm,  $\delta r = \delta z = 0.1$  cm
- Poisson solver tolerance  $EPS = 10^{-10}$ , fluid definition:  $\mu_0 = 10$  Pa.s,  $\rho = 1000$  kg m<sup>-3</sup>,  $\lambda_1 = 0.01$ .
- Scaling parameters:  $L = R = 0.01$  m,  $U = 1$  ms<sup>-1</sup>. Hence,  $Re = 1$  and  $We = 1$ .

To demonstrate that the technique presented in this paper can cope with viscoelastic fluids governed by the Oldroyd-B model, we used the data above and performed three simulations. The first simulation we set  $\lambda_2 = 0.9\lambda_1$ ; in the second simulation a value of  $\lambda_2 = 0.5\lambda_1$  was employed, in the third simulation we chose  $\lambda_2 = 0.1\lambda_1$ . We observe that the value of  $We = 1$  used in these simulations is not the effective Weissenberg number. The effective Weissenberg number for the Oldroyd-B model, as pointed out by Yoo and Na [1], is

$$We_{\text{effect}} = \left(1 - \frac{\lambda_2}{\lambda_1}\right) We.$$

Thus, in these simulations we used  $We_{\text{effect}} = 0.1, 0.5, 0.9$ , respectively. The results of the simulations are displayed in figure 5. Figure 5 shows different time frames of the jet flowing through the tube and then being extruded into the air. The swelling ratio  $S_r = D_{max}/L$  is also shown. For the time  $t = 5.0$  the jet is just leaving the tube and the differences between the three cases are small. However, as the jet is extruded into the air the differences become noticeable as we can see by comparing the size of the jet swelling for the three cases. As expected, the maximum swell occurs for the case of  $We_{\text{effect}} = 0.9$ .

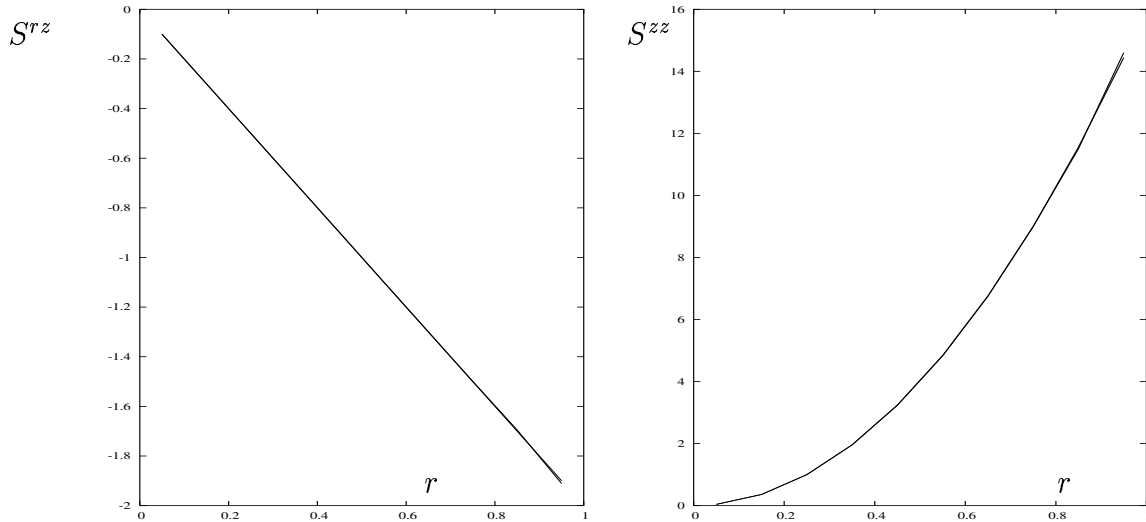


**Fig. 4.** Numerical and analytical solutions of  $S^{rz}$  and  $S^{zz}$  at time  $t = 25$  at the position  $z = 5$ . The dotted-dashed line represents the numerical solution. The solid lines represent the exact solutions given by (44).

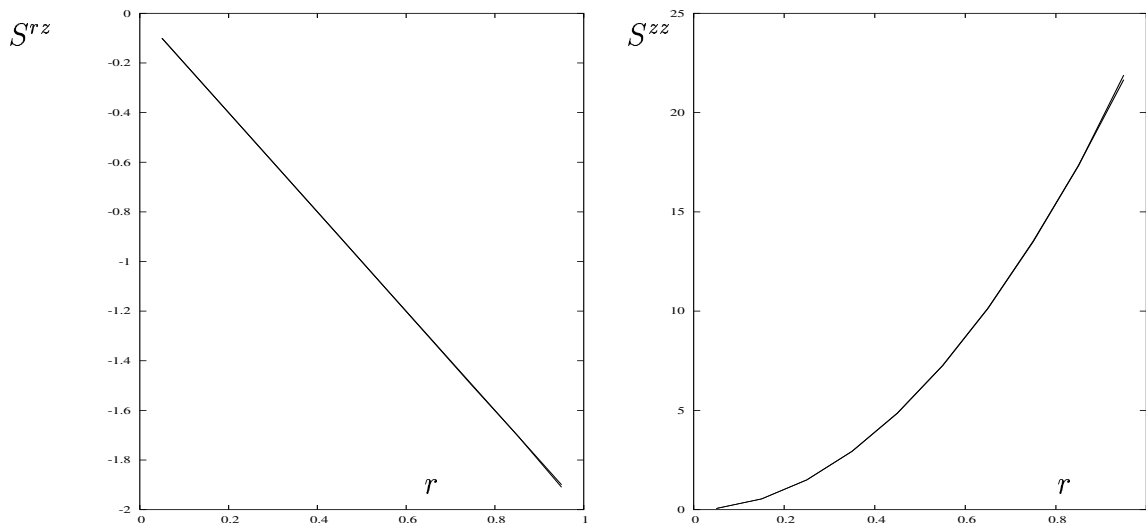


**Fig. 5.** Numerical and analytical solutions of  $S^{rz}$  and  $S^{zz}$  at time  $t = 25$  at the position  $z = 5$ . The dotted-dashed line represents the numerical solution. The solid lines represent the exact solutions given by (44).

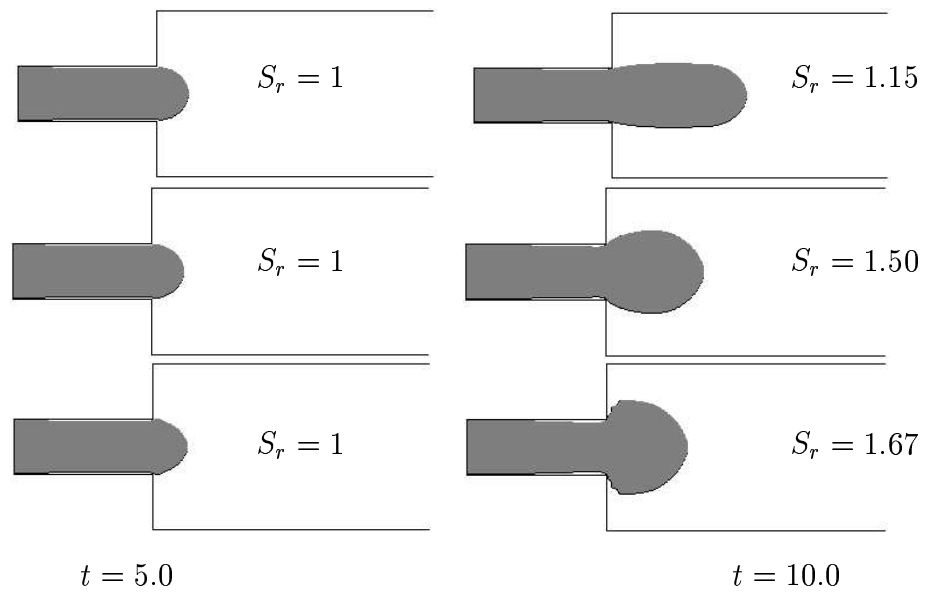


**Fig. 6.** Numerical simulation of the extrudate swell of an axisymmetric jet for  $We_{\text{effect}} = 0.1, 0.5, \text{ and } 0.9$ . Fluid flow visualization at different times. At time  $t = 5.0$  the swelling ratio is  $S_r = 1$  (as the jet is leaving the tube and entering the air).

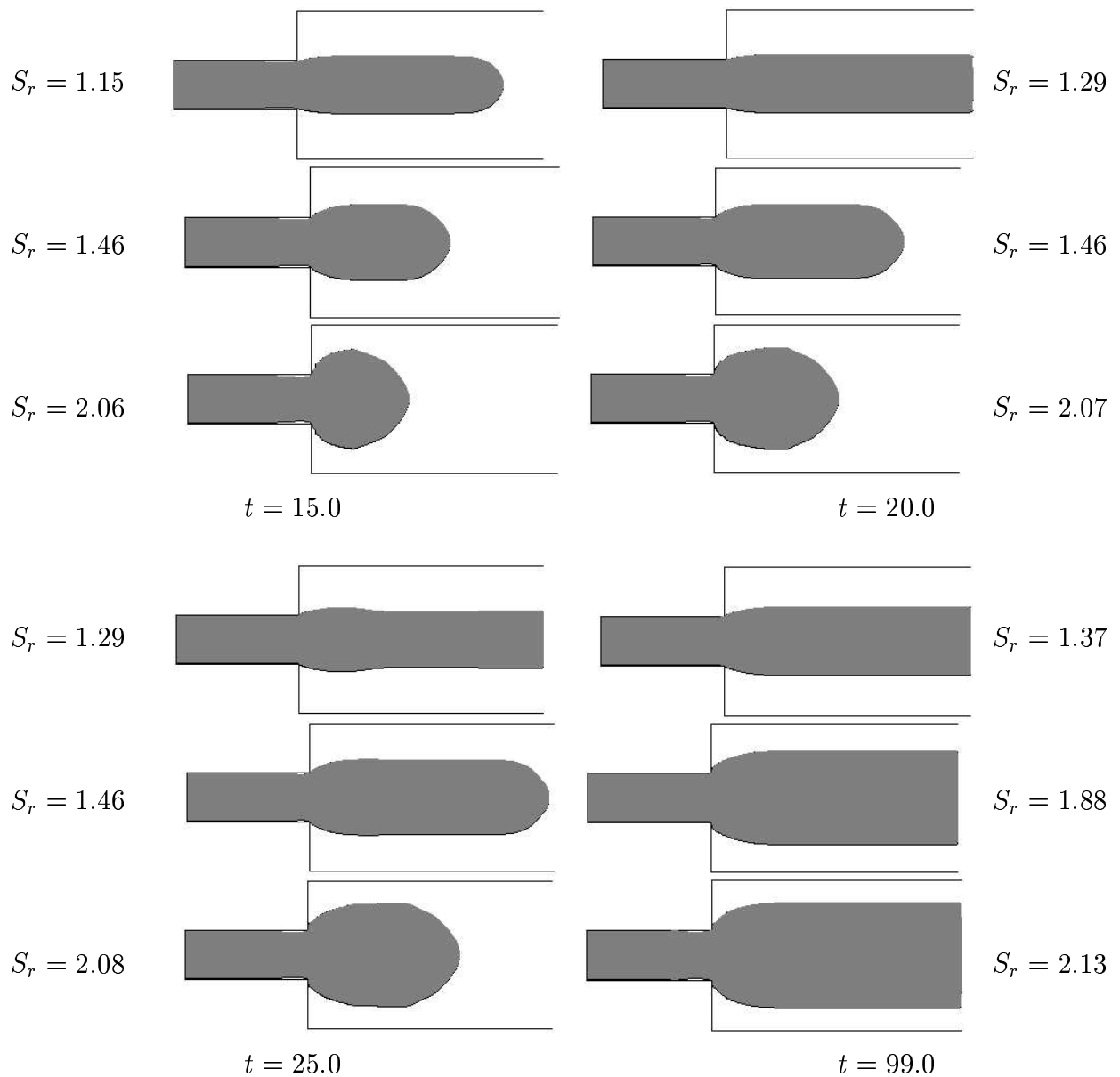


**Fig. 6.** Continued.

## 7. Conclusions

We presented a numerical technique for simulating unsteady viscoelastic free surface flows of an Oldroyd-B fluid. The finite difference method described in this paper is an extension of the two-dimensional method introduced by (Tomé et al. 2002) to axisymmetric free surface flows. The main features of this work is the computation of the non-Newtonian extra stress components on rigid boundaries, on the symmetry axis as well as the treatment of the free surface stress conditions. The numerical method has been validated by simulating pipe flow for several values of the Weissenberg number and compared to the respective exact solution. To demonstrate that this technique can cope with viscoelastic free surface flows we simulated the transient extrudate swell of an axisymmetric jet governed by the Oldroyd-B model. We used Weissenberg numbers of  $We_{effect} = 0.1, 0.5$  and  $0.9$  and obtained swelling ratios of 37%, 88% and 113%, respectively. These results agree with experimental observations and demonstrates that the numerical technique presented in this paper can cope with highly elastic fluids.

## Acknowledgements

We gratefully acknowledge support given by Fundação de Amparo a Pesquisa do Estado de São Paulo (Fapesp proc. no. 00/03385-0) and Conselho Nacional de Pesquisa (CNPq).

## References

- Amsden, A.A. & Harlow, F.H., 1970, "The SMAC method: a numerical technique for calculating incompressible fluid flow", Los Alamos Scientific Laboratory, Report LA-4370.
- Batchelor, G.K., 1967, "An Introduction to Fluid Dynamics", Cambridge University Press, Cambridge.
- Beris, A.N., Armstrong, R.C., Brown, R.A., 1987, "Spectral finite-element calculations of the flow of a Maxwell fluid between eccentric rotating cylinders", *J. Non-Newtonian Fluid Mech.*, vol. 22, pp. 129-167.
- Brasseur, E., Fyrrillas, M.M., Georgiou, G.C., Crochet, M.J., 1998, "The time-dependent extrudate-swell problem of an Oldroyd-B fluid with slip along the wall", *J. Rheol.* vol. 42, No. 3, pp. 549-566.
- Crochet, M.J., Keunings R., 1980, "Die swell of a Maxwell fluid– numerical prediction", *J. Non-Newtonian Fluid Mech.*, vol. 7, pp. 199-212.
- Crochet, M.J., Keunings, R., 1982, "Finite element analysis of die swell of a highly elastic fluid", *J. Non-Newtonian Fluid Mech.*, vol. 10, pp. 339-356.
- Crochet, M., Davis, A.R., Walters, K., 1984, "Numerical Simulation of Non-Newtonian Flow", Elsevier, New York.
- Carew, E.O.A., Townsend, P. and Webster, M.F., 1993, "A Taylor-Petrov-Galerkin algorithm for viscoelastic flow", *J. Non-Newtonian Fluid Mech.* vol. 50, pp. 253-287.
- Huang, X., Phan-Thien, N., Tanner, R.I., 1996, "Viscoelastic flow between eccentric rotating cylinders: Unstructured control volume method", *J. Non-Newtonian Fluid Mech.* vol. 64, pp. 71-92.
- Keunings, R., Crochet, M.J., 1984, "Numerical Simulation of a viscoelastic fluid through an abrupt contraction", *J. Non-Newtonian Fluid Mech.* vol. 14, pp. 279-299.
- Marchal, J.M., Crochet, M.J., 1987, "A new mixed finite element for calculating viscoelastic flow", *J. Non-Newtonian Fluid Mech.* vol. 26, pp. 77-114.
- Mompean, G., Deville, M., 1997, "Unsteady finite volume of Oldroyd-B fluid through a three-dimensional planar contraction", *J. Non-Newtonian Fluid Mech.*, vol. 72, pp. 253-279.
- Phan-Thien, N., Tran-Cong T. Graham A.L., 1991, "Shear flow of periodic arrays of particle clusters: A boundary element method", *J. Fluid Mech.*, vol. 228 (5), pp. 275-293.
- Phillips, T.N. and Williams, A.J., 1999, "Viscoelastic flow through a planar contraction using a semi-Lagrangian finite volume method", *J. Non-Newtonian Fluid Mech.*, vol. 87, pp. 215-246.
- Purnode, B., Crochet, M.J., 1987, "Flows of polymer solutions through contractions. Part 1: flows of polyacrylamide solutions through planar contractions", *J. Non-Newtonian Fluid Mech.* vol. 65, pp. 269-289.
- Tomé, M.F., Mangiavacchi, N., Cuminato, J.A., Castelo, A. McKee, S., 2002, "A finite difference technique for simulating unsteady viscoelastic free surface flows", *J. Non-Newtonian Fluid Mech.*, vol. 106, pp. 61-106.
- Tomé, M.F., Duffy, B.R., McKee, S., 1996, "A numerical technique for solving non-Newtonian free surface flows, *J. Non-Newtonian Fluid Mech.*", vol. 62, pp. 9-34.
- Tome, M. F., McKee, S., 1994, "GENSMAC: A Computational Marker-and-Cell Method for Free Surface Flows in General Domains", *Journal of Computational Physics*, vol. 110, pp. 171-186.
- Ferreira, V.G., Tomé, M.F., Mangiavacchi, N., Castelo, A., Cuminato, J.A., Fortuna, A., McKee, S., 2002, "High Order Upwinding and the Hydraulic Jump", *Int. J. Numer. Methods Fluids*, vol. 39, pp. 549-583.
- Xue, S.C., Phan-Thien, N., Tanner, R.I., 1998, "Three-dimensional numerical simulation of viscoelastic flows through planar contractions", *J. Non-Newtonian Fluid Mech.*, vol. 74, pp. 195-245.
- Yoo, J.Y., Na, Y., 1991, "A numerical study of the planar contraction flow of a viscoelastic fluid using the SIMPLER algorithm", *J. Non-Newtonian Fluid Mech.* vol. 30, pp. 89-106.